

# Soft X-ray spectroscopy study of the electronic structure of oxidized and partially-oxidized magnetite nanoparticles

*Benjamin Gilbert\*<sup>1</sup>, Jordan E. Katz<sup>1</sup>, Jonathan D. Denlinger<sup>2</sup>, Yadong Yin<sup>3</sup>, Roger Falcone<sup>2</sup> and Glenn  
A. Waychunas<sup>1</sup>*

<sup>1</sup>Earth Science Division, Lawrence Berkeley National Laboratory, Berkeley CA 94720.

<sup>2</sup>Advanced Light Source, Lawrence Berkeley National Laboratory, Berkeley CA 94720.

<sup>3</sup>Department of Chemistry, University of California, Riverside, CA 92521.

\*To whom correspondence should be addressed: [BGilbert@lbl.gov](mailto:BGilbert@lbl.gov)

ABSTRACT The crystal structure of magnetite nanoparticles may be transformed to maghemite by complete oxidation, but under many relevant conditions the oxidation is partial, creating a mixed valence material with structural and electronic properties that are poorly characterized. We used X-ray diffraction, Fe K-edge extended X-ray absorption fine structure (EXAFS) spectroscopy and soft X-ray absorption and emission spectroscopy to characterize the products of oxidizing uncoated and oleic-acid-coated magnetite nanoparticles in air. The oxidization of uncoated magnetite nanoparticles creates a material that is structurally and electronically indistinguishable from maghemite. By contrast, while oxidized oleic-acid-coated nanoparticles are also structurally indistinguishable from maghemite, Fe L-edge spectroscopy revealed the presence of interior reduced iron sites even after a 2-year period. We used X-ray emission spectroscopy at the O K-edge to study the valence bands (VB) of the iron oxide nanoparticles, using resonant excitation to remove the contributions from oxygen atoms in the ligands and from low-energy excitations that obscured the VB edge. The bonding in all nanoparticles was typical of maghemite, with no detectable VB states introduced by the long-lived, reduced-iron sites in the oleic-acid-coated sample. However, O K-edge absorption spectroscopy observed a  $\sim 0.2$  eV shift in the position of the lowest unoccupied states in the coated sample, indicating an increase in the semiconductor band gap relative to bulk stoichiometric maghemite that was also observed by optical absorption spectroscopy. The results show that the ferrous iron sites within ferric iron oxide nanoparticles coated by an organic ligand can persist under ambient conditions with no evidence of a distinct interior phase, and exert an effect on the global electronic and optical properties of the material. This phenomenon resembles the band gap enlargement caused by electron accumulation in the conduction band of  $\text{TiO}_2$ .

## Introduction

The oxidation of iron oxide nanoparticles of the magnetite ( $\text{Fe}_3\text{O}_4$ ) phase, which contains both divalent and trivalent iron atoms, is a common pathway for the formation of nanoparticles of the

maghemite ( $\gamma\text{Fe}_2\text{O}_3$ ) phase, a fully trivalent iron oxide. This pathway is harnessed for the production of iron oxide nanoparticles for technological purposes. In a typical synthesis, nanoparticles of the ferrous iron oxide wustite,  $\text{Fe(II)O}$ , are formed through the thermal decomposition of iron pentacarbonyl,  $\text{Fe(CO)}_5$  and reaction with the surfactant oleic acid at high temperature. These nanoparticles transform into magnetite,  $\text{Fe(II)Fe(III)}_2\text{O}_4$ , and subsequently to maghemite,  $\gamma\text{-Fe(III)}_2\text{O}_3$  by oxidation.<sup>1, 2, 3</sup> Maghemite nanoparticles produced in this way are of interest as building blocks of functional arrays for electronic and optical applications,<sup>4, 5</sup> for their ability to perform as drug delivery systems and superparamagnetic contrast enhancement agents,<sup>6</sup> and to provide both solid support and photoelectrically active centers for photocatalytic processes.<sup>7, 8</sup>

The oxidation of magnetite nanoparticles is also an important process in environmental settings. Magnetite nanoparticles can be formed by microbial activity in anaerobic subsurface regions and subsequently oxidized to maghemite following exposure to  $\text{O}_2$  or aqueous oxidants.<sup>9</sup> This process is a component of important environmental redox cycles that couple the chemistry of iron, carbon and numerous other elements to the microbial ecology of soils and sediments. In addition, magnetite oxidation is relevant to environmental applications of zerovalent iron (ZVI) nanoparticles, which can be effective for the reductive transformation of environmental contaminants such as chlorinated hydrocarbons and arsenic<sup>10, 11</sup> but which are rapidly oxidized upon exposure to air. Magnetite is the first oxidation product, forming either an exterior shell<sup>12</sup> or hollow oxide nanocrystals due to the nanoscale Kirkendall effect.<sup>13, 14</sup> Further oxidation leads to the formation of a ferric oxide surface layer that reduces the effective reactivity of the nanomaterials.

In both technological and environmental settings, then, the behavior of oxidized magnetite nanoparticles is dependent upon the structural and chemical properties of the transformed nanoparticles. Numerous studies have found that the oxidation of bulk and nanoscale magnetite is frequently incomplete, forming a partially oxidized and poorly defined end product.<sup>15-18</sup> Magnetite is an inverse spinel with  $\text{Fe}^{2+}$  and  $\text{Fe}^{3+}$  cations distributed among octahedral sites and  $\text{Fe}^{3+}$  cations at tetrahedral sites.

During oxidation to maghemite the crystal topology and morphology are conserved as ferrous iron cations diffuse from the interior to the surface where they are oxidized.  $\text{Fe}^{2+}$  diffusion leaves vacant octahedral sites that ensure charge conservation as the stoichiometry changes to the final phase that is written as  $\text{Fe}_{2(1-\frac{1}{3}\square)}\text{O}_{3(2-\frac{2}{3}\square)}$ , where  $\square$  represents the cation vacancy (ref. 19). At ambient  $p\text{O}_2$ , magnetite is thermodynamically unstable but its oxidation can be kinetically hindered by the activation barrier for ferrous iron diffusion to the surface. Because oxidation requires diffusion through the crystal, the rate and extent of oxidation is strongly dependent on particle size, and studies have found that nanoparticles with stoichiometries intermediate between pure magnetite or maghemite can be formed that are metastable in air.<sup>16,20</sup>

Despite the many studies of magnetite oxidation, obtaining an accurate description of the structure and chemical properties of the oxidized products remains a considerable challenge. In related research, we have shown that ultrafast X-ray methods can track the fate of transient ferrous iron sites created in maghemite nanoparticles with the goal of measuring the kinetics of this pathway for environmental iron redox cycling.<sup>21</sup> However, lack of a complete description of such materials impedes data interpretation and model development. Here we report an investigation into the structure, oxidation state and electronic properties of such maghemite nanoparticles formed via the oxidation of magnetite nanoparticles, in particular combining soft x-ray absorption and emission spectroscopy to characterize the electronic structure around the band gap.

## Experimental Methods

*Nanoparticle and bulk reference synthesis.* Oleic acid coated iron oxide nanoparticles were synthesized through the thermal decomposition of  $\text{Fe}(\text{CO})_5$  in organic solvents and subsequent oxidation in air.<sup>22, 23</sup> In a typical synthesis, 0.2 mL of  $\text{Fe}(\text{CO})_5$  was added to a mixture containing 10 mL octyl ether and 1.44 mL oleic acid at 100°C under argon flow. The resulting mixture was agitated vigorously using a magnetic stirrer, while the solution was heated to 295°C and kept at that temperature for 1 h. During this process, the initial orange color of the solution gradually turned from brown to black. The

solution was then cooled down to 200°C and bubbled with air for 2 h. Finally, the solution was cooled down to room temperature. Excess ethanol was added to the solution to precipitate the sample, which was then collected by centrifugation. The resulting black powder was finally redispersed into 10.0 ml toluene. Transmission electron microscopy indicated that oxidation did not lead to the formation of hollow spheres.<sup>13</sup>

Uncoated magnetite nanoparticles were synthesized using an aqueous precipitation method under oxygen-free conditions in which particle size is controlled by solution pH and ionic strength.<sup>24</sup> Briefly, 0.808g of Fe(III)(NO<sub>3</sub>)<sub>3</sub>, 0.252 g of Fe(II)(ClO<sub>4</sub>)<sub>2</sub>·xH<sub>2</sub>O and 0.085 – 0.256 g of NaNO<sub>3</sub> were dissolved in 1 mL ultra pure water immediately prior to synthesis to create solutions with a nominal ferrous:ferric ratio of 2:1. This mixture was added by a peristaltic pump at a constant rate to a rapidly stirred solution of NaNO<sub>3</sub> at a predetermined concentration (1M, 2M or 3M) and pH (11 or 12). The pH of the solution was maintained ±0.1 pH units. The magnetic black nanoparticles were cleaned of excess ions by dialysis against ultrapure water for five days, then dried at room temperature in air forming a brown powder.

Bulk crystalline magnetite reference was synthesized following a standard method.<sup>25</sup> After verifying the phase and phase purity with conventional X-ray powder diffraction a portion of dried magnetite powder was transformed to bulk crystalline maghemite by heating at 170°C in air for two days.

*X-ray diffraction.* We performed powder x-ray diffraction (XRD) at the Advanced Light Source (ALS), Lawrence Berkeley National Laboratory, beamline 11.3.1 to determine unit cell parameters and estimate the particle size of bulk and nanoscale iron oxides. Bulk references and uncoated iron oxide nanoparticles were studied as dry powders were mounted on Kapton tape and XRD was performed in transmission using a two-dimensional (2D) charge coupled device (CCD) detector. The scattering geometry was calibrated using a LaB<sub>6</sub> standard and the 2D data were integrated using Fit2D. Instrument resolution was estimated using a NIST silicon standard. XRD data were analyzed using the MAUD code to refine unit cell parameters as well as particle size. Following thermal oxidation and annealing, the bulk maghemite samples exhibited vacancy ordering reducing the symmetry from *cubic* to *tetragonal*,

and we refined the data using space group  $P4_3212$ .<sup>19, 26</sup> However, this symmetry reduction cannot be identified in the nanoparticle data due to peak width broadening, and the XRD data were refined using space group  $P4_332$ .

*X-ray absorption spectroscopy at the iron K-edge.* We acquired room temperature x-ray absorption near-edge structure (XANES) and x-ray absorption extended fine structure (EXAFS) spectra from bulk and nanocrystalline iron oxides to investigate the chemical oxidation state of iron and the local coordination geometry, respectively. The data were acquired at beamline 10-2 at the Stanford Synchrotron Radiation Laboratory (SSRL) with the monochromator de-tuned to 50% intensity to reduce the contribution from higher harmonic x-rays. The dried powder samples were mixed with boron nitride, mounted between Kapton tape and measured in transmission using an iron foil standard for energy calibration. Data reduction was performed in the Athena module of the IFEFFIT code.

*Soft x-ray spectroscopy at the oxygen K- and iron L-edges.* Bulk and nanocrystalline iron oxides were studied with soft x-ray absorption and emission spectroscopy (XAS and XES) at the oxygen K-edge to reveal electronic structure of the valence and conduction bands. Portions of finely ground bulk and dried nanoparticle samples were pressed into indium foil for analysis under vacuum. Because oleic acid exhibits a high vapor pressure it was not practical to perform studies of the unbound ligand. Oxygen K-edge x-ray absorption and resonant x-ray emission studies were performed at beamlines 7.0 and 8.0 at the ALS. The incident x-ray energy resolution was set to approximately 0.2 eV and 0.35 eV for absorption and emission spectroscopy, respectively. The x-ray emission spectrometer has a resolution of about 0.5 eV<sup>27</sup>. Fe L-edge absorption spectroscopy was performed at ALS beamline 7.0 with the incident energy resolution set to 0.3 eV, acquiring the fluorescence and electron yield signals simultaneously.

O K-edge absorption spectra were acquired in fluorescence yield and were calibrated by applying a linear transformation to the energy axis to align the spectrum obtained from a  $\text{TiO}_2$  (anatase) standard to a published reference<sup>28</sup>. The absolute energy calibration of the emission x-ray spectrometer was

determined with reference to the Zn L<sub>2,3</sub> emission lines from a zinc metal standard. The absorption spectra were normalized for the energy dependence of incident beam intensity by the division of a gold grid electron yield signal acquired simultaneously with the sample, and then scaled to unity step jump at 552.5 eV. The XES spectra were normalized to a constant maximum intensity.

## Results

We used a combination of transmission electron microscopy (TEM), x-ray absorption spectroscopy (XAS) and x-ray diffraction (XRD) to investigate the iron oxidation state, crystal phase and particle size of the air-oxidized nanoparticles. The OA-coated nanoparticles dispersed easily onto a TEM grid for imaging (**Fig. 1**) but no images of non-aggregated uncoated nanoparticles could be obtained. Fe K-edge XAS provides information on iron oxidation state through the energy position of the onset of the main edge<sup>29</sup>, with the ferrous iron component in bulk magnetite shifting the edge position by 1.4 eV to lower energy than bulk maghemite, as shown in **Figure 2a**. The absorption edge position of all air-oxidized nanoparticles was indistinguishable from that of bulk maghemite. Fe K-edge XAS can additionally distinguish the magnetite and maghemite crystal phases because differences in the local iron-oxygen coordination affect the lineshape in the extended X-ray absorption fine structure (EXAFS) region and its Fourier transform (**Figs. 2b & c**, respectively).<sup>12, 29, 30</sup> Comparison with bulk references showed that for all air-oxidized nanoparticles the local iron coordination is typical of that observed in the maghemite phase. The XRD patterns displayed in **Figure 3** exhibit significant peak width broadening caused by small particle size. As a consequence, XRD cannot distinguish between the maghemite and magnetite phases in nanoparticles,<sup>12</sup> but particle size may be estimated by fitting the data with the maghemite structure (**Table 1**). In accordance with prior observations, the size of nanoparticles synthesized by the aqueous synthesis method is controlled by solution pH and ionic strength<sup>24</sup>.

Several features of the data of **Figs. 2 and 3** indicate that the nanoparticles exhibit considerable variation in crystallinity. Specifically, the samples differ in the relative sharpness of features in the Fe K-edge XAS near-edge region (**Fig. 2a**) and the apparent coordination number of neighboring atoms

lying outside the first shell (**Fig. 2c**), both of which are affected by structural disorder. These observations are broadly consistent with the results of full-profile Reitveld refinement of the XRD data assuming a *cubic* maghemite structure summarized in **Table 1**. The oleic acid (OA) coated nanoparticles synthesized at high temperature exhibit the lowest site disorder than any other sample, including the bulk, while exactly matching the bulk cell dimensions.

Oxygen K-edge XAS spectra of transition metal oxides and oxyhydroxide depict the density of states in the conduction band including metal atom states that are accessible due to the covalency of the metal – oxygen bond.<sup>31, 32</sup> **Figures 4** and **5** display oxygen K-edge XAS spectra for bulk magnetite, bulk maghemite and selected nanoparticles. Features in the pre-edge region (530 – 534 eV) represent O *1s* transitions to unoccupied Fe *3d* states that are split by the crystal field of the local distorted octahedral coordination geometry.<sup>33</sup> The onset of pre-edge fine structure observed for bulk magnetite is shifted by 0.25 eV to higher energy relative to bulk maghemite.<sup>12</sup> At higher energies, the lineshape in the multiple scattering (MS) region is sensitive to atomic geometry through the impact of structure on the upper conduction band.<sup>34, 35</sup> Although the spectra from the two phases are very similar, the exact position and strength of the MS resonance around 548 eV is diagnostic of the two phases (see asterisk in **Fig. 5**).

As shown in **Figure 4**, all of the uncoated nanoparticles oxidized in air match the maghemite phase in both pre-edge and MS regions. Loss of lineshape sharpness for the smaller nanoparticles is consistent with increased structural disorder. Loss of pre-edge intensity has been attributed to the reduction of metal atom hybridization<sup>36, 37</sup> or the presence of cation vacancies, and thus a lower net coordination of oxygen by iron.<sup>14, 37</sup>

As shown in **Figure 5**, the O K-edge XAS spectrum of the OA-coated nanoparticles acquired in surface sensitive total electron yield (TEY) mode is dominated by the signal from oxygen atoms in the oleic acid surfactant while the fluorescence yield (FY) signal is a linear combination of oxide and ligand spectra. Comparison of the TEY and FY data shows that the ligand contribution does not interfere with key features in the FY spectrum attributable to the iron oxide nanoparticles, including the pre-edge onset



position and the MS resonance around 548 eV. The pre-edge onset energy identical to that of the magnetite reference while the MS resonance matches the maghemite reference. This unexpected finding was checked three times over a two-year period to ensure no errors in beamline calibration, with identical results.

Iron *L*-edge XAS is sensitive to iron oxidation state, and has been used to estimate the magnetite/maghemite ratio in mixed-phase nanoparticles.<sup>38</sup> Comparing XAS acquired using the TEY vs. FY signals permits the chemistry of surface vs. interior iron sites to be distinguished.<sup>39</sup> The iron TEY spectrum from OA-coated nanoparticles indicates the surface to be composed of maghemite, but the FY signal reveals a different spectrum originating from the interior (**Fig. 6**). A previous study showed that OA-coated metallic cobalt nanoparticles introduced a distinct metal-to-ligand charge transfer (MLCT) peak in the Cu *L*-edge XAS.<sup>40</sup> However, as no changes to the surface-sensitive TEY Fe *L*-edge spectrum are observed, we conclude that the FY spectrum reveal the presence of reduced iron sites within the interior. However, the FY spectrum cannot be interpreted as a linear combination of maghemite plus either of the reduced phases, magnetite<sup>2</sup> or wüstite.<sup>41</sup>

Non-resonant soft X-ray emission spectroscopy (nr-XES) provides a depiction of the density of states in the valence band of metal oxide semiconductors by analyzing the X-ray photons emitted following metal or oxygen core level excitation above threshold. For semiconductors with completely empty or completely filled *3d* shells, such as CdSe<sup>42</sup> and ZnO,<sup>42, 43</sup> it has been shown that the band gap can be measured as the energy difference between *onset positions* of the O *K*-edge XAS and nr-XES spectra. However, we found this approach to be inaccurate for hematite,  $\alpha\text{Fe}_2\text{O}_3$ , for which the band gap was instead predicted by the energy difference between *threshold positions* of the O *K*-edge XAS and nr-XES spectra, defined as the first inflection point.<sup>37</sup> In **Fig. 7a** we apply this approach to spectra acquired from the bulk maghemite sample, obtaining a band gap of  $2.0 \pm 0.1$  eV, which is in close agreement with the commonly accepted value of 2.04 eV. Also shown is the resonant XES spectrum acquired with the excitation energy tuned to the first peak in the O XAS spectrum (arrow in **Fig. 7a**). For both

maghemite and hematite,<sup>37</sup> we find that tuning the excitation energy closer to threshold removes progressively more intensity from states that appear to lie at the top of the VB. For maghemite and hematite the position of the inflection point is not changed but is revealed more clearly in the first derivative plot.

Magnetite exhibits much higher conductivity than maghemite at room temperature, attributable to a smaller band gap of approximately 0.15 eV. The magnetite VB revealed by XES has a different profile than maghemite and extra structure in the first derivative of the resonant XES is consistent with the presence of a sub-band at the top of the VB that prior resonant PES identified as being derived from the ferrous iron states.<sup>44, 45</sup> The first inflection point of the magnetite resonant XES spectrum is closer in energy to the CB than for maghemite, but the band gap predicted by this method (1.5 eV) is much greater than the literature value. As discussed below, **Fig. 7** shows that while the magnetite and maghemite VB are distinguishable by O K-edge XES, this approach is not able to locate the magnetite VB edge and hence the band gap of this material.

We used XES to investigate the VB of OA-coated nanoparticles (**Fig. 8**). For non-resonant excitation, the emission spectrum contains contributions from oleic acid and iron oxide. The ligand contribution is resonantly enhanced when the excitation energy is tuned to the ligand peak at 531.6 eV but may be reduced or eliminated by lower excitation energies, permitting comparison with the equivalent resonant XES data from the bulk references. As shown in **Fig. 9**, the resonant XES of the OA-coated nanoparticles is a closer match to maghemite than magnetite. The VB threshold position is identical to maghemite although the VB is ~0.5 eV wider. The data from uncoated nanoparticles are an even closer match to maghemite.

Because the O K-edge XAS data implied a difference in the unoccupied electronic structure between the uncoated and OA-coated nanoparticles, we performed optical absorption spectroscopy to seek corresponding effects upon the electronic excitations. In the visible region, the bulk magnetite spectrum (**Fig. 10**) is dominated a broad absorption threshold that is mainly attributed to band gap excitation,

while that of black magnetite nanoparticles is strong and featureless.<sup>46</sup> The visible absorption spectrum of the uncoated nanoparticles closely matches bulk maghemite but a blue shift of  $\sim 50$  nm (0.2 eV) is evident for the OA-coated nanoparticles. This blue shift is similar in sign and magnitude to the difference in O K-edge absorption threshold position between the coated and uncoated nanoparticles. A distinct absorption band at approximately 650 nm seen in the bulk maghemite spectrum is missing for both nanoparticle samples analyzed here, but has been previously observed on larger maghemite nanoparticles<sup>46</sup>. As this feature is typically interpreted as originating from localized *dd* excitations,<sup>47</sup> its apparent dependence on particle size is surprising and warrants further investigation.

## Discussion

### *The electronic structure of oxidized magnetite nanoparticles*

The complementary structural and electronic analyses described above revealed that uncoated magnetite nanoparticles with diameters less than 10 nm are readily oxidized in air forming a phase that is indistinguishable from maghemite. In agreement with our prior study of hematite nanoparticles there is no observed dependence of the electronic structure of this ferric iron oxide with particle diameter in the range 3.5 – 9 nm.

Studies of oleic-acid-coated magnetite nanoparticles revealed more complex behavior. While X-ray methods sensitive to crystal structure also showed that the OA-coated nanoparticles had converted to the maghemite structure following oxygen exposure, Fe L-edge spectroscopy revealed the presence of reduced iron atoms in the interior of the nanoparticles. Although reduced iron sites were not detectable in the near-surface region, their presence caused a global effect on the electronic properties of the nanoparticles with shifts on the order of 0.2 eV observed in both O K-edge X-ray absorption spectra and optical absorption spectra. These data are consistent with an increase in the band gap, with the O XAS data suggesting that the CB position of OA-coated iron oxide nanoparticles is raised relative to bulk maghemite.

Because O K-edge XAS involves electronic transitions between core and valence electronic states,

factors that influence the O 1s core level must be considered in order to rule out alternative interpretations. First, changes in valence electron density in the vicinity of the oxygen atom can affect the ground state 1s binding energy. Such core level chemical shifts are observed in O 1s PES studies of doped manganates,<sup>48</sup> although we are not aware of an equivalent study in the maghemite-magnetite series (in the present case the oleic acid coating prevented the acquisition of O 1s PES data). However, the Fe L-edge XAS data revealed the presence of reduced iron sites. This excess electron density (relative to fully oxidized maghemite) would reduce the O 1s binding energy, and hence also the 1s → CB transition energy, an opposite effect to the one observed.

Second, following core level photoexcitation, the electrostatic field of a core hole can increase the apparent binding energy of the final state DOS.<sup>49</sup> In the present case, excess electron density could shield the core hole, reducing final state binding and effectively raising the observed energy position. However, it is widely accepted that oxygen core holes are completely screened in iron oxides.<sup>31,35,50</sup> In a recent study, the temperature dependence of the magnetite band gap, including both the abrupt change at the Verwey transition temperature and the gradual trend above and below, was detectable by O K-edge XAS.<sup>45</sup> The trend in the XAS onset position directly revealed the contribution of the CB shift to the total band gap change. This study indicates that CB shifts detected by O XAS of iron oxides may be attributed to actual band-edge electronic structure changes. Finally, optical absorption spectroscopy does not involve core-level electrons, and the observation of a blue-shift in these data corroborates our interpretation of shifts observed in the X-ray spectra.

The observation of “charge-trapping” within spinel iron oxides has been previously observed although without a determination of the effect of interior ferrous iron sites on the electronic properties.<sup>51</sup> Our conclusion that incompletely oxidized magnetite nanoparticles exhibit modified band-edge electronic structure is consistent with a recent study that correlated the ferrous iron content of ~10-nm magnetite nanoparticles subjected to varying degrees of oxidation with measurements of their redox potential and the kinetics of interfacial reduction processes.<sup>20</sup> A consistent description of the reduction kinetics was

possible only if the ferrous iron content affected the thermodynamics for interfacial electron transfer – i.e., the effective energy positions of band-edge states. Moreover, our findings resemble the Burstein shift observed in TiO<sub>2</sub> nanocrystalline electrodes in which potentiostat-controlled electron transfer to the TiO<sub>2</sub> nanoparticles causes a reversible increase in the optical band gap.<sup>52</sup> This effect is typically interpreted as representing the filling of the lowest CB levels although debate remains as to the nature of the states that are filled (e.g., localized surface trap states vs. extended CB levels) and to the contribution of cation adsorption following electron transfer that may additionally modulate the positions of electronic states.<sup>53</sup> Although the CB states in titania vs. iron oxides differ in their symmetry and localization, it is plausible that our findings represent a chemical version of the Burstein shift. Direct reproduction of this effect in iron oxide nanoparticle electrodes would be challenging in aqueous solution due to the expected loss of ferrous ions by dissolution, but studies in a non-aqueous medium are planned.

### ***The physical structure of oxidized magnetite nanoparticles***

The data suggest that the structure of incompletely oxidized magnetite nanoparticles is more complex than a core-shell structure composed of two fully-stoichiometric phases. In particular, the interior-sensitive Fe L-edge spectra are not consistent with the presence of a discrete magnetite phase. In fact, the exceedingly close agreement in Fe K-edge XANES and EXAFS spectra for OA-coated nanoparticles and the maghemite reference precludes the existence of any substantial second phase including magnetite, FeO or Fe<sup>0</sup>. The determination of realistic structural models of such complex nanoparticles will require the creative combination of approaches including X-ray scattering techniques, molecular modeling and electron microscopy.

The comparison between uncoated and oleic-acid-coated nanoparticles of approximately the same dimensions illustrates the role of the surface ligand in limiting magnetite oxidation. As a passive covering, the ligand may simply hinder O<sub>2</sub> diffusion to the oxide surface. Alternatively, ligand-oxide bonding may enhance the activation barrier for the diffusion of ferrous iron sites to the surface. The

latter effect could conceivably permit arbitrarily long stabilization of structural ferrous iron within small iron oxide nanoparticles but further studies are required to determine the dominant mechanism.

### ***Band Gap Measurements in Transition Metal Oxides by Soft-X-ray Spectroscopy***

As shown above, photon-in/photon-out X-ray spectroscopy is a versatile approach for studying the electronic properties of both bulk and nanoscale semiconductor materials, including ligand-coated nanoparticles. However, in all iron oxides studied by this approach, O K-edge XES detects an energy-dependent spectral weight at and above the VB edge that lowers the apparent band gap.<sup>37, 54, 55</sup> For magnetite in particular this effect makes the edge of the VB impossible to locate, in contrast to the clearer determination achieved by VB PES.<sup>45, 55</sup> The excess intensity in the O XES data is enhanced as the photon energy is tuned above threshold but the position of the spectral weight on the emission energy axis is dispersionless (i.e., it does not move with the excitation energy). In our previous study of hematite, similar observations were interpreted as representing normal X-ray fluorescence of an indirect gap semiconductor. However, this interpretation relies upon the validity of band theory to describe the electronic structure of iron oxides, which remains uncertain given the localized nature of the Fe *3d* electrons, so here we seek an alternative explanation. The dispersionless behavior of the band edge intensity is not consistent with a coherent resonant inelastic X-ray scattering (RIXS) process in which the two-photon excitation and decay process is coupled to a lower-energy electronic transition.<sup>57</sup> Instead, it could represent a shake-up process in which valence electron excitations are stimulated during the relaxation of a core-level electron promoted by an X-ray photon to a state above the top of the CB. In this picture, the excess XES intensity is caused by normal fluorescence transitions from the excited states. The energy scale of the shake up excitations is less than the band gap; therefore the excitations are likely the same low-energy *dd* excitations that cause structure in the sub-band-gap region of the optical absorption spectra of transition metal oxides. Discrete shake up transitions with energy scales of 2 – 7 eV have been identified in resonant x-ray emission spectroscopy studies at transition metal K-edges.<sup>56</sup>

A soft-X-ray-based method of band gap determination in transition metal oxide nanoparticles would be a valuable complement to approaches based on optical absorption or spectroelectrochemistry. An alternative approach for band gap determination is to seek the RIXS energy-loss feature that represents the lowest energy excitation of a valence electron above the band gap. Band gap excitations of transition metal oxide semiconductors involve partially occupied  $3d$  states, and such  $dd$  transitions are typically strong features in metal L-edge emission spectroscopy of these materials.<sup>57</sup> However, in recent studies this approach underestimated the band gap for  $\text{Fe}_2\text{O}_3$  (refs. 57, 58) and  $\text{FeO}$  (ref. 41) by about 0.1 eV. Since core hole effects do not perturb the low-energy transitions studied by RIXS spectroscopy, this discrepancy is not understood and represents current uncertainty as to the accuracy with which X-ray spectroscopy can determine the excitation energies in transition metal oxides.

## Conclusions

We have shown that ferrous iron sites within ferric iron oxide nanoparticles coated by an organic ligand can persist under ambient conditions with no evidence of a distinct interior phase, and can exert an effect on the global electronic and optical properties of the material. This demonstrates the value of X-ray spectroscopic methods of characterizing the electronic properties and mixed-valence nanomaterials created by partial oxidation or reduction processes, which remain challenging to characterize and to predict. Because metal oxide nanoparticles composed of redox-active transition metals such as iron are environmentally relevant and have the potential to perform or catalyze technologically useful redox reactions through interfacial electron transfer, more work is required to connect the electronic properties and consequent chemical reactivity of electrons in redox-active transition metal oxides.

ACKNOWLEDGMENT Soft X-ray spectroscopy was performed on beamlines 7 and 8 at the Advanced Light Source (ALS), and we thank Pers-Anders Glans and Jinghua Guo. X-ray diffraction was performed on beamline 11.3.3 at the ALS, and we thank Simon Teat. The ALS is supported by the Director, Office of Science, Office of Basic Energy Sciences, of the U.S. Department of Energy (DOE)

under Contract No. DE-AC02-05CH11231. Iron K-edge absorption spectroscopy was performed at beamline 10-2 at the Stanford Synchrotron Radiation Lightsource (SSRL), a national user facility operated by Stanford University on behalf of the DOE Office of Basic Energy Sciences, and we thank Matthew Lattimer and Allyson Aranda. We thank Rebecca Mezler, Pupa Gilbert and Jinghua Guo for the opportunity to acquire Fe L-edge data, and Klaus Attenkofer and David Sherman for valuable discussions. This work was supported by the Director, Office of Science, of the U.S. Department of Energy under Contract No. DE-AC02-05CH11231.

#### SUPPORTING INFORMATION PARAGRAPH None

1. Redl, F. X.; Black, C. T.; Papaefthymiou, G. C.; Sandstrom, R. L.; Yin, M.; Murray, C. B.; O'Brien, S. P., Magnetic, Electronic and Structural Characterization of Nonstoichiometric Iron Oxides at the Nanoscale. *Journal of the American Chemical Society* **2004**, *126*, 14583-14599.
2. Ge, J. P.; Hu, Y. X.; Biasini, M.; Dong, C. L.; Guo, J. H.; Beyermann, W. P.; Yin, Y. D., One-step synthesis of highly water-soluble magnetite colloidal nanocrystals. *Chemistry-a European Journal* **2007**, *13* (25), 7153-7161.
3. Corias, A.; Mountjoy, G.; Loche, D.; Puentes, V. F.; Falqui, A.; Zanella, M.; Parak, W. J.; Casula, M. F., Identifying spinel phases in nearly monodisperse iron oxide colloid nanocrystal. *Journal of Physical Chemistry C* **2009**, *113*, 18667-18675.
4. Lee, S.; Fursina, A.; Mayo, J. T.; Yavuz, C. T.; Colvin, V. L.; Sofin, R. G. S.; Shvets, I. V.; Natelson, D., Electrically driven phase transition in magnetite nanostructures. *Nature Materials* **2008**, *7* (2), 130-133.
5. Rybchenko, S. I.; Dyab, A. K. F.; Haywood, S. K.; Itskevich, I. E.; Paunov, V. N., Strained arrays of colloidal nanoparticles: conductance and magnetoresistance enhancement. *Nanotechnology* **2009**, *20* (42).
6. Martina, M. S.; Fortin, J. P.; Menager, C.; Clement, O.; Barratt, G.; Grabielle-Madellmont, C.; Gazeau, F.; Cabuil, V.; Lesieur, S., Generation of superparamagnetic liposomes revealed as highly efficient MRI contrast agents for in vivo imaging. *Journal of the American Chemical Society* **2005**, *127* (30), 10676-10685.
7. Milone, C.; Ingoglia, R.; Schipilliti, L.; Crisafulli, C.; Neri, G.; Galvagno, S., Selective hydrogenation of alpha,beta-unsaturated ketone to alpha,beta-unsaturated alcohol on gold-supported iron oxide catalysts: Role of the support. *Journal of Catalysis* **2005**, *236* (1), 80-90.
8. Fröba, M.; Köhn, R.; Bouffaud, G.; Richard, O.; Tendeloo, c., Fe<sub>2</sub>O<sub>3</sub> nanoparticles within mesoporous MCM-48 silica: In situ formation and characterization. *Chemistry of Materials* **1999**, *11*, 2858-2865.
9. Lovley, D. R.; Stolz, J. F.; Nord, G. L.; Phillips, E. J. P., Anaerobic production of magnetite by a dissimilatory iron-reducing microorganism. *Nature* **1987**, *330* (6145), 252-254.
10. Wang, Z., Nanoscale iron particles for environmental remediation: An overview. *Journal of Nanoparticle Research* **2003**, *5*, 323-332.
11. Kanel, S. R.; Manning, B.; Charlet, L.; Choi, H., Removal of arsenic(III) from groundwater by nanoscale zero-valent iron. *Environmental Science & Technology* **2005**, *39* (5), 1291-1298.
12. Signorini, L.; Pasquini, L.; Savini, L.; Carboni, R.; Boscherini, F.; Bonetti, E.; Giglia, A.; Pedio, M.; Mahne, N.; Nannarone, S., Size-dependent oxidation in iron/iron oxide core-shell nanoparticles.



*Physical Review B* **2003**, 68.

13. Cabot, A.; Puentes, V. F.; Shevchenko, E.; Yin, Y.; Balcells, L.; Marcus, M. A.; Hughes, S. M.; Alivisatos, A. P., Vacancy coalescence during oxidation of iron nanoparticles. *Journal of the American Chemical Society* **2007**, 129 (34), 10358-+.
14. Wang, C.; Baer, D. R.; Amonette, J. E.; Engelhard, M. H.; Antony, J.; Qiang, Y., Morphology and electronic structure of the oxide shell on the surface of iron nanoparticles. *Journal of the American Chemical Society* **2009**, 131, 8824-8832.
15. Gallagher, K. J.; Feitknecht, W.; Mannweiler, U., Mechanism of oxidation of magnetite to  $\gamma$ -Fe<sub>2</sub>O<sub>3</sub>. *Nature* **1968**, 217, 1118-1121.
16. Tang, J.; Myers, M.; Bosnik, K. A.; Brus, L. E., Magnetite Fe<sub>3</sub>O<sub>4</sub> nanocrystals: Spectroscopic observation of aqueous oxidation kinetics. *Journal of Physical Chemistry B* **2003**, 107, 7501-7506.
17. Jolivet, J. P.; Tronc, E., Interfacial electron transfer in colloidal spinel iron-oxide - Conversion of Fe<sub>3</sub>O<sub>4</sub> -  $\gamma$ -Fe<sub>2</sub>O<sub>3</sub> in aqueous medium. *Journal of Colloid and Interface Science* **1988**, 125 (2), 688-701.
18. Sidhu, P. S.; Gilkes, R. J.; Posner, A. M., Mechanism of the low temperature oxidation of magnetite. *Journal of Inorganic and Nuclear Chemistry* **1977**, 39, 1953-1958.
19. Greaves, C., A powder neutron diffraction investigation of vacancy ordering and covalence in  $\gamma$ -Fe<sub>2</sub>O<sub>3</sub>. *Journal of Solid State Chemistry* **1983**, 49, 325-333.
20. Gorski, C. A.; Nurmi, J. T.; Tratnyek, P. G.; Hofstetter, T. B.; Scherer, M. M., Redox Behavior of Magnetite: Implications for Contaminant Reduction. *Environmental Science & Technology* **2010**, 44 (1), 55-60.
21. Katz, J. E.; Gilbert, B.; Zhang, X.; Attenkofer, K.; Falcone, R. W.; Waychunas, G. A., Time-resolved X-ray spectroscopy of ferrous iron formation in dye-sensitized maghemite nanoparticles. *Journal of Physical Chemistry Letters* **2010**, Submitted.
22. Hyeon, T.; Lee, S. S.; Park, J.; Chung, Y.; Bin Na, H., Synthesis of highly crystalline and monodisperse maghemite nanocrystallites with a size-selection process. *Journal of the American Chemical Society* **2001**, 123, 12798-12801.
23. Zhang, T. R.; Ge, J. P.; Hu, Y. P.; Yin, Y. D., A general approach for transferring hydrophobic nanocrystals into water. *Nano Letters* **2007**, 7, 3203-3207.
24. Vayssieres, L.; Chanéac, C.; Tronc, E.; Jolivet, J. P., Size Tailoring of Magnetite Particles Formed by Aqueous Precipitation: An Example of Thermodynamic Stability of Nanometric Oxide Particles *Journal of Colloid and Interface Science* **1998**, 205, 205-212.
25. Schwertmann, U.; Cornell, R. M., *Iron Oxides in the Laboratory: Preparation and Characterization*. Wiley-VCH: Verlag, 2000.
26. Pecharromás, C.; González-Carreno, T.; Iglesias, J. E., The infrared dielectric properties of maghemite,  $\gamma$ -Fe<sub>2</sub>O<sub>3</sub>, from reflectance measurement on pressed powders. *Physics and Chemistry of Minerals* **1995**, 22, 21-29.
27. Nordgren, J.; Nyholm, R., Design of a portable large spectral range grazing-incidence instrument. *Nuclear Instruments and Methods A* **1986**, 246, 242-245.
28. Lusvardi, V. S.; Barteau, M. A.; Chen, J. G.; Eng, J., Jr.; Frühberger, B.; Tplyakov, A., An NEXAFS investigation of the reduction and reoxidation of TiO<sub>2</sub>(001). *Surface Science* **1998**, 397, 237-250.
29. Wilke, M.; Farges, F.; Petit, P.-E.; Brown, G. E., Jr.; Martin, F., Oxidation state and coordination of Fe in minerals: An Fe K-XANES spectroscopic study. *American Mineralogist* **2001**, 86 (714-730).
30. Chen, L. X.; Liu, T.; Thurnauer, M. C.; Csencsits, R.; Rajh, T., Nanoparticle Structures Investigated by X-ray Absorption Near-Edge Structure, Surface Modifications, and Model Calculations. *Journal of Physical Chemistry B* **2002**, 106, 8539-8546.
31. de Groot, F. M. F.; Grioni, M.; Fuggle, J. C.; Ghijssen, J.; Sawatzky, G. A.; Petersen, H., Oxygen 1s x-ray-absorption edges of transition-metal oxides. *Physical Review B* **1989**, 40.
32. van Aken, P. A.; Liebscher, B.; Styrsa, V. J., Core level electron energy-loss spectra of minerals:

- pre-edge fine structures at the oxygen K-edge. *Physics and Chemistry of Minerals* **1998**, *25*, 494-498.
33. Sherman, D. M., Electronic structures of iron(III) and manganese(IV) (hydr)oxide minerals: Thermodynamics of photochemical reductive dissolution in aquatic environments. *Geochimica Cosmochimica Acta* **2005**, *69*, 3249-3255.
  34. Wu, Z. Y.; Gota, S.; Jollet, F.; Pollak, M.; Gautier-Soyer, M., Characterization of iron oxides by x-ray absorption at the oxygen K edge using a full multiple-scattering approach *Physical Review B* **1997**, *55*, 2570-2577.
  35. Mackrodt, W. C.; Joliet, F.; Gautier-Soyer, M., A first principles Hartree-Fock interpretation of the X-ray oxygen K-edge spectrum of haematite ( $\alpha$ -Fe<sub>2</sub>O<sub>3</sub>). *Philosophical Magazine B* **1999**, *79*, 25-36.
  36. Kuiper, P.; van Elp, J.; Sawatzky, G. A.; Fujimori, A.; Hosoya, S.; de Leeuw, D. M., Unoccupied density of state of La<sub>2-x</sub>Sr<sub>x</sub>NiO<sub>4+d</sub> studied by polarization-dependent x-ray-absorption spectroscopy and bremsstrahlung isochromate spectroscopy. *Physical Review B* **1991**, *44* (4570-4575).
  37. Gilbert, B.; Frandsen, C.; Maxey, E.; Sherman, D. M., Soft x-ray spectroscopy studies of the electronic structure of hematite nanoparticles. *Phys Rev B* **2009**, *79*.
  38. Park, J.; An, K.; Hwang, Y.; Park, J.-E.; Noh, H.-J.; Kim, J.-Y.; Park, J.-H.; Hwang, N.-M.; Hyeon, T., Ultra-large-scale syntheses of monodisperse nanocrystals. *Nature Materials* **2004**, *3*, 891-895.
  39. Kuepper, K.; Raekers, M.; Taubitz, C.; Hesse, H.; Neumann, M.; Young, A. T.; Piamonteze, C.; Bondino, F.; Prince, K. C., Fe valence state of Sr<sub>2</sub>FeMoO<sub>6</sub> probed by x-ray absorption spectroscopy: The sample age matters. *J. Appl. Phys.* **2008**, *104* (3), 3.
  40. Liu, H.; Guo, J.; Yin, Y.; Augustsson, A.; Dong, C.; Nordgren, J.; Chang, C.; Alivisatos, A. P.; Thornton, G.; Ogletree, D. F.; Requejo, F. G.; de Groot, F. M. F.; Salmeron, M., Electronic structure of cobalt nanocrystals suspended in liquid. *Nano Letters* **2007**, *7*, 1919-1922.
  41. Prince, K. C.; Matteucci, M.; Kuepper, K.; Chiuzbaian, S. G.; Bartowski, S.; Neumann, M., Core-level spectroscopic study of FeO and FeS<sub>2</sub>. *Physical Review B* **2005**, *71*.
  42. Lüning, J.; Rockenberger, J.; Eisbitt, S.; Rubensson, J. E.; Karl, A.; Kornowski, A.; Weller, H.; Eberhardt, W., Soft X-ray spectroscopy of single sized CdS nanocrystals: size confinement and electronic structure. *Solid State Communications* **1999**, *112*, 5-9.
  43. Dong, C. L.; Persson, P.; Vayssieres, L.; Augustsson, A.; Schmitt, T.; Mattesini, M.; Ahuja, R.; Chang, C. L.; Guo, J.-H., Electronic structure of nanostructured ZnO from x-ray absorption and emission spectroscopy and the local density approximation. *Physical Review B* **2004**, *70*.
  44. Lad, R. J.; Henrich, V. E., Photoemission study of the valence-band electronic structure in Fe<sub>x</sub>O<sub>x</sub>, Fe<sub>3</sub>O<sub>4</sub>, and  $\alpha$ -Fe<sub>2</sub>O<sub>3</sub> single crystals. *Physical Review B* **1989**, *39*, 13478-13485.
  45. Park, J.-H.; Tjeng, L. H.; Allen, J. W.; Metcalf, P.; Chen, C. T., Single-particle gap above the Verwey transition in Fe<sub>3</sub>O<sub>4</sub>. *Physical Review B* **1997**, *55*, 12813-12817.
  46. He, Y. P.; Miao, Y. M.; Li, C. R.; Wang, S. Q.; Cao, L.; Xie, S. S.; Yang, G. Z.; Zou, B. S.; Burda, C., Size and structure effect on optical transitions of iron oxide nanocrystals. *Physical Review B* **2005**, *71*.
  47. Sherman, D. M.; Burns, R. G.; Burns, V. M., Spectral characteristics of the iron oxides with application to the Martian bright region mineralogy. *Journal of Geophysical Research* **1982**, *87*, 10169-10180.
  48. Park, J.-H.; Chen, C. T.; Cheong, S.-W.; Bao, W.; Meigs, G.; Chakarian, V.; Idzerda, I., Electronic aspects of the ferromagnetic transition in manganese perovskites. *Physical Review Letters* **1996**, *76*, 4215-4218.
  49. de Groot, F. M. F., High-resolution X-ray emission and X-ray absorption spectroscopy. *Chemical Reviews* **2001**, *101*, 1779-1808.
  50. van Elp, J.; Tanaka, A., Threshold electronic structure at the oxygen K edge of 3 d -transition-metal oxides: A configuration interaction approach. *Physical Review B* **1999**, *60*.
  51. McCormick, M. L.; Adriaens, P., Carbon tetrachloride transformation on the surface of

- nanoscale biogenic magnetite particles *Environmental Science & Technology* **2004**, 38, 1045-1053.
52. Rothenberger, G.; Fitzmaurice, D.; Grätzel, M., Spectroscopy of Conduction Band Electrons in Transparent Metal Oxide Semiconductor Films: Optical Determination of the Flatband Potential of Colloidal Titanium Dioxide Films. *Journal of Physical Chemistry* **1992**, 96, 5983-5986.
53. Boschloo, G.; Fitzmaurice, D., Electron accumulation in nanostructured TiO<sub>2</sub> (anatase) electrodes. *Journal of Physical Chemistry B* **1999**, 103, 7860-7868.
54. Prince, K. C.; Bondino, F.; Zangrando, M.; Zaccagna, M.; Kuepper, K.; Neumann, M.; Parmigiani, F., Dichroic O 1s photoabsorption and resonant X-ray scattering in haematite (Fe<sub>2</sub>O<sub>3</sub>). *Journal of Electron Spectroscopy and Related Phenomena* **2005**, 144-147, 719-722.
55. Moewes, A.; Kurnmaev, E. Z.; Finkelstein, L. D.; Galakhov, A. V.; Gota, S.; Gautier-Soyer, M.; Rieff, J. P.; Hague, C. F., X-ray emission spectroscopy study of the Verwey transition in Fe<sub>3</sub>O<sub>4</sub>. *Journal of Physics: Condensed Matter* **2003**, 15, 2017-2022.
56. Lu, L.; Hancock, J. N.; Chabot-Couture, G.; Ishii, K.; Vajk, O. P.; Yu, G.; Mizuki, J.; Casa, D.; Gog, T.; Greven, T., Incident energy and polarization-dependent resonant inelastic x-ray scattering study of La<sub>2</sub>CuO<sub>4</sub>. *Physical Review B* **2006**, 74.
57. Duda, L.-C.; Nordgren, J.; Drager, G.; Bocharov, S.; Kirchner, T., Polarized resonant inelastic X-ray scattering from single-crystal transition metal oxides. *Journal of Electron Spectroscopy and Related Phenomena* **2000**, 110-111, 275-285.
58. Moewes, A.; Kurmaev, E. Z.; Finkelstein, L. D.; Galakhov, A. V.; Gota, S.; Gautier-Soyer, M.; Rueff, J. P.; Hague, C. F., X-ray emission spectroscopy study of the Verwey transition in Fe<sub>3</sub>O<sub>4</sub>. *Journal of Physics: Condensed Matter* **2003**, 15, 2017-2022.

# FIGURES

## Soft X-ray spectroscopy study of the electronic structure of oxidized and partially-oxidized magnetite nanoparticles

*Benjamin Gilbert\*<sup>1</sup>, Jordan E. Katz<sup>1</sup>, Jonathan D. Denlinger<sup>2</sup>, Roger Falcone<sup>2</sup>, Yadong Yin<sup>3</sup> and Glenn  
A. Waychunas<sup>1</sup>*

<sup>1</sup>Earth Science Division, Lawrence Berkeley National Laboratory, Berkeley CA 94720.

<sup>2</sup>Advanced Light Source, Lawrence Berkeley National Laboratory, Berkeley CA 94720.

<sup>3</sup>Department of Chemistry, University of California, Riverside, CA 92521.

Sample	Bulk	Oleic	Uncoated					
	$\gamma\text{Fe}_2\text{O}_3$	OA	6	8	9	10	11	13
pH			12	11	12	11	12	11
[ $\text{NNO}_3$ ]			3	3	2	2	1	1
D(NM)	>100	6.1(1)	3.2	3.5	3.5	4.2	4.4	9.2
a (Å)	8.3278	8.3278	8.32819	8.32909	8.3312	8.3220	8.3278	8.30948
$B(\text{Fe}_1 \text{ oct}) (\text{Å}^2)$	3.0	1.7	2.8	3.1	2.7	3.6	3.0	3.1
$B(\text{Fe}_2) (\text{Å}^2)$	"	"	"	"	"	"	"	"
$B(\text{Fe}_3 \text{ tet}) (\text{Å}^2)$	16.5	7.5	16.0	14.9	21.6	17.4	16.5	8.8
$B(\text{O}_1) (\text{Å}^2)$	2.9	0.9	3.4	3.6	3.2	3.2	2.9	2.2
$B(\text{O}_2) (\text{Å}^2)$	"	"	"	"	"	"	"	"

**Table 1.** Maghemite unit cell parameters and particle size obtained from fits to x-ray diffraction data.

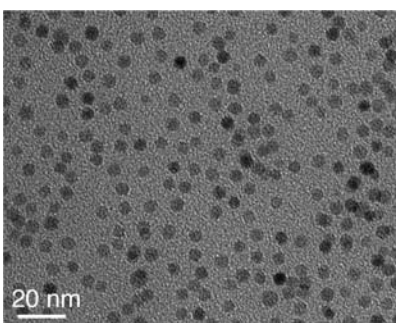


**Figure 1** Transmission electron microscopy image of oleic acid coated maghemite nanoparticles.

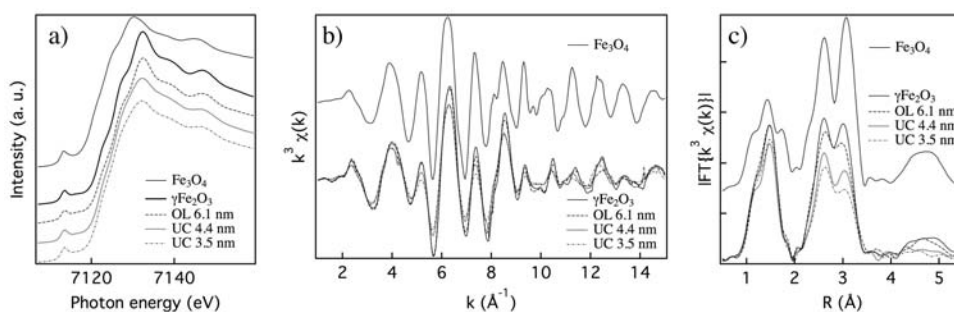


**Figure 2** (a) Iron K-edge x-ray absorption spectroscopy of bulk maghemite ( $\gamma\text{-Fe}_2\text{O}_3$ ) and magnetite ( $\text{Fe}_3\text{O}_4$ ) reference materials, and uncoated (UC) and oleic acid (OA) coated iron oxide nanoparticles. (a) Near-edge spectra (b)  $k^3$ -weighted EXAFS  $\chi(k)$  function (c) Magnitude of the EXAFS Fourier transform.

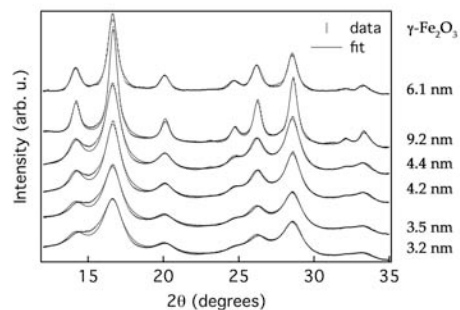


**Figure 3** X-ray diffraction patterns (vertical markers) from magnetite ( $\text{Fe}_3\text{O}_4$ ) iron oxide nanoparticles oxidized to the maghemite ( $\gamma\text{-Fe}_2\text{O}_3$ ) phase. Best-fit results of Reitveld refinement of the maghemite structure to the experimental data are given as solid lines.

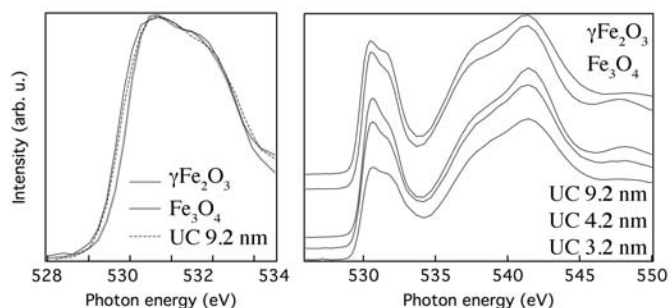


**Figure 4** Oxygen K-edge X-ray absorption spectroscopy from bulk maghemite ( $\gamma\text{-Fe}_2\text{O}_3$ ), magnetite ( $\text{Fe}_3\text{O}_4$ ) and three samples of uncoated (UC) iron oxide nanoparticles. **Left** Detail of pre-edge region acquired in fluorescence yield. **Right** Full spectra acquired in total electron yield.

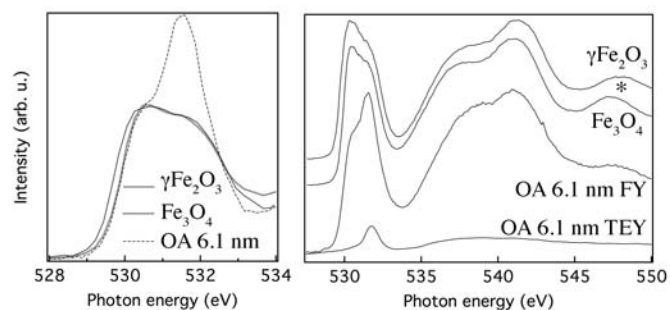


**Figure 5** Oxygen K-edge X-ray absorption spectroscopy from bulk maghemite ( $\gamma\text{-Fe}_2\text{O}_3$ ), magnetite ( $\text{Fe}_3\text{O}_4$ ) and oleic acid (OA) coated nanoparticles. **Left** Detail of pre-edge region acquired in fluorescence yield. **Right** Full spectra acquired in fluorescence yield (FY), except the lowest curve that is acquired in total electron yield (TEY) as discussed in the text. The surface-sensitive TEY signal is dominated by the oleic acid coating. The energy position of the multiple scattering resonance indicated by the asterisk is different for magnetite vs. maghemite.

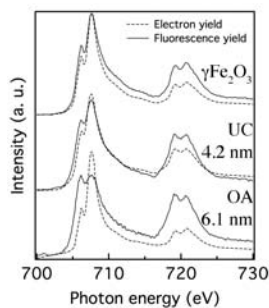


**Figure 6** Iron L-edge X-ray absorption spectra from bulk maghemite ( $\gamma\text{-Fe}_2\text{O}_3$ ) and uncoated (UC) and oleic acid (OA) coated nanoparticles. For each sample, the electron yield (more surface sensitive) and fluorescence yield (less surface sensitive) signals were acquired simultaneously.

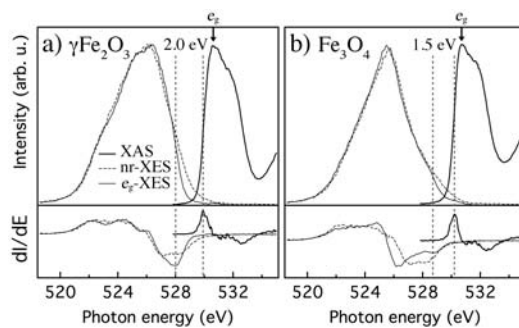


**Figure 7** Oxygen K-edge X-ray absorption spectroscopy (XAS) and X-ray emission spectroscopy (XES) from (a) bulk maghemite ( $\gamma\text{-Fe}_2\text{O}_3$ ) and (b) magnetite ( $\text{Fe}_3\text{O}_4$ ). Non-resonant (n.r.) XES (solid thin lines) were acquired with 560-eV excitation; resonant XES (dashed thin lines) were acquired with photon energy tuned to the first peak labeled  $e_g$ , the symmetry designation of the first unoccupied  $3d$  state of octahedrally-coordinated high-spin ferric iron. The first derivatives of the spectrum intensities with respect to photon energy are given beneath, using consistent line styles. The position of the first inflection points of the  $e_g$ -XES and XAS data are indicated by vertical dashed lines, and the energy gap is displayed.

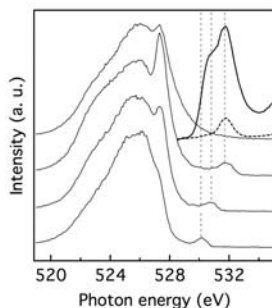


**Figure 8** Oxygen K-edge X-ray absorption spectroscopy (XAS) and X-ray emission spectroscopy (XES) from 6.1-nm oleic acid coated iron oxide nanoparticles. The top, non-resonant XES spectrum was acquired with 560-eV excitation and the lower resonant XES spectra were acquired at photon energies indicated by vertical dashed lines. XAS data acquired in both fluorescence and total electron yield are given (c.f. caption to Figure 4).

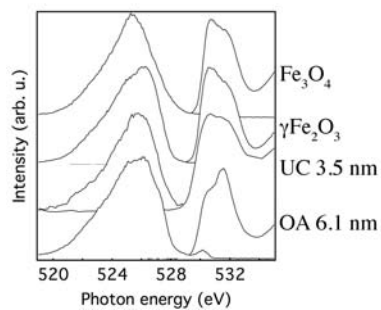


**Figure 9** Summary of oxygen K-edge X-ray absorption spectroscopy (XAS) and resonance X-ray emission spectroscopy (XES) acquired with threshold excitation for bulk references and coated and uncoated iron oxide nanoparticles.

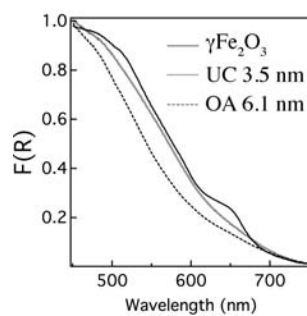


**Figure 10** The Kubelka-Munk functions,  $F(R)$ , of powders of bulk and nanoparticulate maghemite obtained from UV-visible spectroscopy performed in the diffuse reflectance mode.



## **DISCLAIMER**

This document was prepared as an account of work sponsored by the United States Government. While this document is believed to contain correct information, neither the United States Government nor any agency thereof, nor the Regents of the University of California, nor any of their employees, makes any warranty, express or implied, or assumes any legal responsibility for the accuracy, completeness, or usefulness of any information, apparatus, product, or process disclosed, or represents that its use would not infringe privately owned rights. Reference herein to any specific commercial product, process, or service by its trade name, trademark, manufacturer, or otherwise, does not necessarily constitute or imply its endorsement, recommendation, or favoring by the United States Government or any agency thereof, or the Regents of the University of California. The views and opinions of authors expressed herein do not necessarily state or reflect those of the United States Government or any agency thereof or the Regents of the University of California.